Journal of Sound and Vibration (2002) **250**(4), 723–744
doi:10.1006/jsvi.2001.3940, available online at http://www.idealibrary.com on IDEAL®

MODEL COMPARISON FOR ACOUSTIC SCATTERING BY A SPHERICAL AIR BUBBLE IN WATER

C.-C. WANG AND Z. YE

Wave Phenomena Laboratory, Department of Physics, National Central University, Chung-li, Taiwan 32054, *Republic of China. E-mail: zhen@phy.ncu.edu.tw*

(*Received* 22 *June* 2000, *and in final form* 16 *August* 2001)

The oscillation of a bubble has many vibrational modes, contributing to different portions in acoustic scattering. Without approximations *a priori*, an hydrodynamic approach is applied to investigate acoustic scattering by a bubble in water, taking into account the heat exchange and viscosity. The scattering function is derived for a wide range of frequencies. Examples are shown to illustrate the thermal and viscous effects on sound scattering. Comparison is made with three existing models. While these models are known not to be applicable for high frequencies, it is shown here that even in the low-frequency region, there are also noticeable discrepancies between the exact solution and the three existing models with regard to the scattering properties such as the scattering cross-section, and the quality factor of resonant peaks. By numerical simulation, we claim that the discrepancies may be due to the incomplete consideration of the thermal exchange process in the previous models. The approach presented here is valid for any other fluid enclosure in liquids.

1. INTRODUCTION

Acoustic scattering by a spherical air bubble in liquids has been studied intensively over the past years, as it plays a significant role in a variety of situations of great interest, such as wave propagation in upper ocean surfaces, generation of ambient noise in the ocean, and modelling sound scattering by fish [1–11]. When a bubble is much smaller than the wavelength, the acoustic scattering is dominated by the pulsating mode, and the scattering function can be approximated as isotropic and is given by [9]

$$f_0 = \frac{R_0}{(\omega_0^2(\omega)/\omega^2) - 1 - 2\mathrm{i}(\beta_a + \beta_v + \beta_t)/\omega}, \tag{1}$$

where R_0 is the bubble radius at equilibrium, ω_0 is the effective natural frequency of bubble vibration, ω is the driving frequency, and β_a, β_v, β_t refer to the damping constants due to the acoustic radiation, viscous, and thermal effects respectively.

In the early works, the thermal and viscous effects were neglected [8, 9]. Later, it was recognized that the sound attenuation due to bubbles in water is very important and the attenuation is contributed significantly by the thermal and viscous effects. This stimulated extensive studies of the energy dissipation by bubbles [2, 4–7]. The main approximations in the previous research are as follows. (1) Only pulsatory vibration of the bubble is considered. (2) The pressure is assumed to be uniform inside the bubble, i.e., the inertia of the gas is negligible. (3) The temperature of the bubble wall remains unchanged during

0022-460X/02/090723 + 22 $35.00/0

pulsation, i.e., the thermal conductivity and heat capacity of the surrounding liquids are assumed to be infinite. These approximations were necessary perhaps because of the following reasons. First, it had been difficult to include thermal and viscous effects in higher order modes. Second, the complexity involved in the dynamics of the gas–liquid interaction made it almost impossible to express the results in an explicit form. Third, in most practical cases, higher order modes are negligible. Due to these limitations, the formula expressed in equation (1) has been restricted to low-frequency acoustic scattering.

From the scientific point of view, however, the understanding of the problem is never complete. The parametric validity of the presumptions made in previous works has not yet been justified by an exact approach. Because of this, an exact solution for the bubble scattering, incorporating all damping effects in all vibrational modes, is highly desirable. Not only that, the recent research has showed that in a number of applications such as Albunex bubbles [12], higher order modes do show some significance, particularly for not too low frequencies. Furthermore, an exact solution can serve as a building block in the study of more complicated situations. With the progress of modern experimental techniques for manipulating a single bubble, the accurate reexamination of the problem of acoustic scattering by a bubble becomes possible. All these motivated us to study the problem further. Unlike previous approaches, we will not make any approximation *a priori*; instead we attempt to solve the problem rigorously.

In this paper, the principles of fluid mechanics are used to derive a complete set of equations which determines the acoustic scattering by a single gas-filled bubble in water. The formulation is exact and valid for any frequency and takes into account the thermal and viscous effects in all vibrational modes. For the special case of low-frequency scattering, numerical results are compared with three existing models, namely, Devin's model [4] and two models from references [2, 3]. The organization of the paper is as follows. In section 2, we derive the exact solution, then briefly review and summarize different approaches and results. In section 3, some numerical comparison is shown. The paper is concluded by a brief summary in section 4.

2. THEORIES

In this section, we first present the exact approach. Then the key concepts and approximations in three previous models will be briefly reviewed. To make a direct comparison, we re-arrange the physical quantities in the three models in terms of the definitions and notations in the present work.

2.1. EXACT THEORY

The sound scattering by a fluid object can be studied rigorously from the fluid mechanics. We follow the approach in references [13, 14] to derive an exact formula for the scattering function of a bubble in boundless liquids incorporating the thermal and viscous damping effects. In the long-wavelength limit, we cast the formula in a form similar to equation (1), from which the damping constants and the effective natural frequency are identified.

As the bubbly liquid consists of both gas and liquid phases, the conservation laws, including momentum, mass and energy conservation, should be satisfied in the two phases separately. The momentum conservation is given by [14]

$$\frac{\partial(\rho v_i)}{\partial t} + \frac{\partial \Pi_{ik}}{\partial x_k} = 0, \tag{2}$$

where ρ is the fluid density. In the above, $\Pi_{ik} = \rho v_i v_k - \sigma_{ik}$ is momentum flux density tensor. The term $\rho v_i v_k$ is from mass transfer and σ_{ik} is the stress tensor including both shear and normal stresses given by

$$\sigma_{ik} = -p\delta_{ik} + \mu\left(\frac{\partial v_i}{\partial x_k} + \frac{\partial v_k}{\partial x_i} - \frac{2}{3}\frac{\partial v_j}{\partial x_j}\delta_{ik}\right), \tag{3}$$

where $\mathbf{v}$ is the fluid velocity, p is the pressure, μ is the shear viscosity, and a summation over repeated indices is implied. The conservation law of mass is described by

$$\frac{\partial \rho}{\partial t} + \frac{\partial(\rho v_i)}{\partial x_i} = 0. \tag{4}$$

The heat energy transfer is governed by [14]

$$\rho T\left(\frac{\partial s}{\partial t} + v_i\frac{\partial s}{\partial x_i}\right) = (\sigma_{ik} + p\delta_{ik})\frac{\partial v_i}{\partial x_k} + \frac{\partial}{\partial x_i}\left(\kappa\frac{\partial T}{\partial x_i}\right), \tag{5}$$

where T is the absolute temperature, s is the specific entropy, κ is the thermal conductivity. Equation (5) states that the heat gain or loss in a unit fluid volume, i.e., the term on the left-hand side, results from the viscosity and thermal exchange represented by the two terms on the right-hand side. Equations (2), (4), and (5) contain five scalar components with seven unknown quantities ($\rho, s, T, \mathbf{v}, p$). To solve for these quantities, two additional thermodynamic relations determining the state of the fluid must be invoked [15]:

$$\mathrm{d}\rho = (\gamma/c^2)\,\mathrm{d}p - (\alpha\rho)\,\mathrm{d}T, \tag{6}$$

and

$$\mathrm{d}s = (c_p/T)\,\mathrm{d}T - (\alpha/\rho)\,\mathrm{d}p, \tag{7}$$

where γ is the ratio of specific heats, c is the adiabatic sound speed, c_p is the specific heat at constant pressure, and α is the volume thermal expansion coefficient of the fluid defined as $\alpha = -(1/\rho)(\partial\rho/\partial T)_p$.

For an incident wave of small amplitude, we can linearize the above equations by writing

$$\rho = \rho_0 + \rho^{(1)},\ s = s_0 + s^{(1)},\ p = p_0 + p^{(1)},\ T = T_0 + T^{(1)}, \tag{8}$$

and for the initially static fluid

$$\mathbf{v} = \mathbf{v}^{(1)}, \tag{9}$$

where the quantities with subscript "0" refer to the physical quantities at equilibrium and those with superscript "(1)" denote the perturbed physical quantities. Substituting equations (8) and (9) with equations (6) and (7) into equations (2)–(5), the linearized expressions are derived as

$$\rho_0\frac{\partial \mathbf{v}^{(1)}}{\partial t} = -\nabla p^{(1)} + \mu_0\nabla^2\mathbf{v}^{(1)} + \frac{\mu_0}{3}\nabla(\nabla\cdot\mathbf{v}^{(1)}), \tag{10}$$

$$\frac{\partial p^{(1)}}{\partial t} = \frac{c_0^2\rho_0}{\gamma_0}\left(\alpha_0\frac{\partial T^{(1)}}{\partial t} - \nabla\cdot\mathbf{v}^{(1)}\right), \tag{11}$$

and

$$\nabla^2 T^{(1)} - \frac{1}{\chi_0}\frac{\partial T^{(1)}}{\partial t} = -\frac{\alpha_0 T_0}{\kappa_0}\frac{\partial p^{(1)}}{\partial t}, \tag{12}$$

where χ_0 is the thermal diffusivity defined as $\kappa_0/\rho_0 c_{p0}$.

The velocity field can be further decomposed into a compressional scalar potential and a rotational vector potential as

$$\mathbf{v}^{(1)} = \nabla\phi^{(1)} + \nabla\times\boldsymbol{\psi}^{(1)}. \tag{13}$$

With an harmonic incident wave of angular frequency ω, equations (10)–(13) become

$$(\nabla^2 + \beta_1)\phi^{(1)} = -\frac{\mathrm{i}\omega\alpha_0}{\beta_3} T^{(1)}, \quad (\nabla^2 + \beta_2) T^{(1)} = \frac{(1-\gamma_0)\beta_1}{\alpha_0\chi_0\gamma_0}\phi^{(1)}, \tag{14}$$

where

$$\beta_1 = \frac{\gamma_0\omega^2}{c_0^2\beta_3}, \; \beta_2 = \frac{\mathrm{i}\omega(\gamma_0 + \beta_3 - 1)}{\chi_0\beta_3\gamma_0}, \; \beta_3 = 1 - \mathrm{i}\frac{4\omega\mu_0\gamma_0}{3\rho_0 c_0^2}, \tag{15}$$

and the Helmholtz equation for the velocity vector potential $\boldsymbol{\psi}^{(1)}$ is

$$(\nabla^2 + k_3^2)\boldsymbol{\psi}^{(1)} = 0, \tag{16}$$

where $k_3 = (1 + \mathrm{i})/\delta_v$ is the viscous wave number, and $\delta_v = \sqrt{2\mu_0/(\rho_0\omega)}$ is the penetration depth of the viscous wave. In the above derivation, the common time factor $\mathrm{e}^{-\mathrm{i}\omega t}$ has been dropped.

To solve equation (14), the normal mode analysis commonly used in solving coupled oscillator problems in classical mechanics should be employed. We seek the solutions in the form

$$\phi^{(1)} = A f_\tau, \quad T^{(1)} = B f_\tau, \tag{17}$$

where f_τ is the Laplacian eigenfunction corresponding to the eigenvalue τ, that is,

$$\nabla^2 f_\tau = \tau f_\tau. \tag{18}$$

Substituting equation (17) into equation (14), the eigenvalue problem can be solved as

$$\tau_{1,2} = -\frac{1}{2}(\beta_1 + \beta_2)\left[1 \mp \sqrt{1 - \frac{4\mathrm{i}\omega\beta_1}{\chi_0\gamma_0(\beta_1 + \beta_2)^2}}\right],$$

$$B_{1,2} = \frac{\mathrm{i}\beta_3}{\alpha_0\omega}(\tau_{1,2} + \beta_{1,2}) A_{1,2}. \tag{19}$$

In addition, the axisymmetric solution to equation (18) in the spherical co-ordinates can be written as

$$f_{\tau_{1n}} = S_n(k_1 r) P_n(\cos\theta),$$

$$f_{\tau_{2n}} = S_n(k_2 r) P_n(\cos\theta), \quad n = 0, 1, 2, \ldots, \tag{20}$$

where S_n is a spherical cylindrical function of order n, P_n is the Legendre polynomial of degree n, $k_{1,2}^2 = -\tau_{1,2}$, and r, θ are co-ordinates of the spherical co-ordinate system (r, θ, ϕ) whose origin is at the center of the bubble and the z- axis lies in the propagation direction of the incident wave.

By equations (19) and (20), the general solutions to the scalar velocity and temperature fields in equation (14) are derived as follows. The velocity scalar potential field is given by

$$\phi^{(1)} = \sum_{n=0}^{\infty} [A_{1n} S_n(k_1 r) + A_{2n} S_n(k_2 r)] P_n(\cos\theta), \tag{21}$$

and the temperature field is written as

$$T^{(1)} = \frac{\mathrm{i}\beta_3}{\omega\alpha_0} \sum_{n=0}^{\infty} [(\beta_1 - k_1^2) A_{1n} S_n(k_1 r) + (\beta_1 - k_2^2) A_{2n} S_n(k_2 r)] P_n(\cos\theta), \tag{22}$$

where A_{1n} and A_{2n} are unknown coefficients to be determined.

As for the solution to equation (16), we can solve it with the following physical considerations. As the system is axisymmetric, the magnitude of the vector function $\boldsymbol{\psi}^{(1)}$ must be independent of azimuthal angle ϕ, and the vector itself points to the azimuthal direction. Therefore, the solution to equation (16) is given by

$$\boldsymbol{\psi}^{(1)} = \hat{e}_\phi \sum_{n=1}^{\infty} C_n S_n(k_3 r) P_n^1(\cos\theta), \tag{23}$$

where $\hat{e}_\phi$ is the azimuthal unit vector of the spherical co-ordinate system, P_n^1 is the associated Legendre polynomial of the first order and degree n, and C_n is an unknown coefficient to be determined.

From equations (21)–(23), we notice that three kinds of waves are involved in the problem. The wavenumbers k_1, k_2 and k_3 correspond to the compressional, thermal and viscous waves respectively. To clarify this, we consider the case where the heat conduction is very small. In this case, the thermal characteristic length scale must be much shorter than the compressional length scale, that is, $|\beta_1| \ll |\beta_2|$. In this limit, with equations (15) and (19), k_1 becomes $k_{1c} = \omega/(c_0\sqrt{\beta_3})$ and k_2 becomes $k_{2c} = (1 + \mathrm{i})/\delta_t$, where $\delta_t = \sqrt{2\chi_0/\omega}$ is the penetration depth of the thermal sound wave. Judging from the forms of k_{1c} and k_{2c}, we know that the former is the wavenumber of sound waves in a fluid; this sound wave is due to the compressibility of the fluid. The latter is the wavenumber of the so-called thermal sound wave. It is known that the thermal sound wave decays more rapidly along the path through the fluid than the compressional sound wave. Therefore, for the usual case that the bubble is placed far away from the acoustic source, the thermal wave incidence caused by thermal conduction from the acoustic source can be neglected. From equations (21)–(23), the choice of S_n depends on the physical conditions. Inside the bubble, the spherical Bessel function of first kind j_n is chosen to avoid divergence, whereas the spherical Hankel function of first kind $h_n^{(1)}$ is chosen for the scattered waves outside the bubble. In this way, the scalar potential for the plane incident wave can be written as

$$\phi_I^{(1)} = \sum_{n=0}^{\infty} A_n j_n(k_1 r) P_n(\cos\theta), \tag{24}$$

where

$$A_n = \varepsilon \mathrm{i}^n (2n + 1), \tag{25}$$

in which ε is the wave amplitude. The incident temperature field is given from equation (22):

$$T_I^{(1)} = \frac{\mathrm{i}\beta_3(\beta_1 - k_1^2)}{\omega\alpha_0} \sum_{n=0}^{\infty} A_n j_n(k_1 r) P_n(\cos\theta). \tag{26}$$

Outside the bubble, the scattering scalar potential from equation (21) is

$$\phi_S^{(1)} = \sum_{n=0}^{\infty} A_n[\alpha_{1n} h_n^{(1)}(k_1 r) + \alpha_{2n} h_n^{(1)}(k_2 r)] P_n(\cos\theta), \tag{27}$$

and the scattering vector potential from equation (23) is derived as

$$\boldsymbol{\psi}_S^{(1)} = \hat{e}_\phi \sum_{n=0}^{\infty} \alpha_{3n} A_n h_n^{(1)}(k_3 r) P_n^1(\cos\theta), \tag{28}$$

and the scattering temperature field is obtained from equation (22) as

$$T_S^{(1)} = \frac{\mathrm{i}\beta_3}{\omega\alpha_0} \sum_{n=0}^{\infty} A_n[(\beta_1 - k_1^2)\alpha_{1n} h_n^{(1)}(k_1 r) + (\beta_1 - k_2^2)\alpha_{2n} h_n^{(1)}(k_2 r)] P_n(\cos\theta). \tag{29}$$

Similarly, for the bubble interior, the scalar potential is written as

$$\tilde{\phi}^{(1)} = \sum_{n=0}^{\infty} A_n[\tilde{\alpha}_{1n} j_n(\tilde{k}_1 r) + \tilde{\alpha}_{2n} j_n(\tilde{k}_2 r)] P_n(\cos\theta), \tag{30}$$

the velocity vector potential field is given by

$$\tilde{\boldsymbol{\psi}}^{(1)} = \hat{e}_\phi \sum_{n=0}^{\infty} \tilde{\alpha}_{3n} A_n h_n^{(1)}(\tilde{k}_3 r) P_n^1(\cos\theta), \tag{31}$$

the temperature field is given by

$$\tilde{T}^{(1)} = \frac{\mathrm{i}\tilde{\beta}_3}{\omega\tilde{\alpha}_0} \sum_{n=0}^{\infty} A_n[(\tilde{\beta}_1 - \tilde{k}_1^2)\tilde{\alpha}_{1n} h_n^{(1)}(\tilde{k}_1 r) + (\tilde{\beta}_1 - \tilde{k}_2^2)\tilde{\alpha}_{2n} h_n^{(1)}(\tilde{k}_2 r)] P_n(\cos\theta), \tag{32}$$

where the tilde denotes the bubble interior.

To determine the unknown coefficients $\alpha_{1,2,3}$ and $\tilde{\alpha}_{1,2,3}$ in equations (27)–(32), we invoke the usual boundary conditions that the velocity, stress, temperature and heat flux are continuous across the bubble surface. These conditions are expressed as

$$v_r^{(1)}|_{r=R_0} = \tilde{v}_r^{(1)}|_{r=R_0}, \tag{33}$$

$$v_\theta^{(1)}|_{r=R_0} = \tilde{v}_\theta^{(1)}|_{r=R_0}, \tag{34}$$

$$[\sigma_{rr}^{(1)} - P_{st} - P_0]|_{r=R_0} = [\tilde{\sigma}_{rr}^{(1)} - \tilde{P}_0]|_{r=R_0}, \tag{35}$$

$$\sigma_{r\theta}^{(1)}|_{r=R_0} = \tilde{\sigma}_{r\theta}^{(1)}|_{r=R_0}, \tag{36}$$

$$T^{(1)}|_{r=R_0} = \tilde{T}^{(1)}|_{r=R_0}, \tag{37}$$

and

$$\left[\kappa_0 \frac{\partial T^{(1)}}{\partial r}\right]_{|r=R_0} = \left[\tilde{\kappa}_0 \frac{\partial \tilde{T}^{(1)}}{\partial r}\right]_{|r=R_0}, \tag{38}$$

where R_0 is the equilibrium bubble radius, $\sigma_{rr}^{(1)}$ and $\sigma_{r\theta}^{(1)}$ are stress tensors in the spherical co-ordinates, P_{st} is the Laplace pressure due to surface tension, P_0 is the hydrostatic pressure in the surrounding liquid, and $\tilde{P}_0$ is the equilibrium gas pressure inside the bubble. As mentioned in reference [16], equations (35) and (36) are not convenient to use. To proceed further, we rewrite them in the following forms:

$$\tilde{\phi}^{(1)} - \frac{\rho_0}{\tilde{\rho}_0}\phi^{(1)} + \frac{2R_0(1-\mu_0/\tilde{\mu}_0)}{\tilde{x}_3^2}\left[2v_r^{(1)} + \frac{1}{\sin\theta}\frac{\partial}{\partial\theta}(v_\theta^{(1)}\sin\theta)\right]$$

$$= (P_0 - \tilde{P}_0 + P_{st})/(\mathrm{i}\omega\tilde{\rho}_0) \quad \text{at } r = R_0, \tag{39}$$

and

$$\tilde{\psi}^{(1)} - \frac{\rho_0}{\tilde{\rho}_0}\psi^{(1)} + \frac{2R_0(1-\mu_0/\tilde{\mu}_0)}{\tilde{x}_3^2}\left(\frac{\partial v_r^{(1)}}{\partial\theta} - v_\theta^{(1)}\right) = 0 \quad \text{at } r = R_0, \tag{40}$$

where $\psi^{(1)}$ and $\tilde{\psi}^{(1)}$ are the magnitude of vector potential $\boldsymbol{\psi}^{(1)}\cdot\hat{e}_\phi$ and $\tilde{\boldsymbol{\psi}}^{(1)}\cdot\hat{e}_\phi$, respectively, and the dimensionless number $\tilde{x}_3$ is given as $\tilde{x}_3 = \tilde{k}_3 a$.

The perturbed surface of the bubble is represented as

$$R(\theta, t) = R_0[1 + X(\theta, t)], \tag{41}$$

where we can expand $X(\theta, t)$ as

$$X(\theta, t) = \mathrm{e}^{-\mathrm{i}\omega t}\sum_{n=0}^{\infty} X_n P_n(\cos\theta). \tag{42}$$

One can derive the expression for P_{st} as

$$P_{st} = \sigma R_0^{-2}[2R_0 + \mathrm{e}^{-\mathrm{i}\omega t}R_0\sum_{n=0}^{\infty}(n-1)(n+2)X_n P_n(\cos\theta)], \tag{43}$$

where σ is the surface tension. In addition, at the gas–liquid interface of the bubble, the radial velocity on either side of the bubble equals the velocity of the surface. Subsequently,

$$\tilde{v}_r^{(1)}|_{r=R_0} = \frac{\partial R(\theta, t)}{\partial t} = R_0\frac{\partial X(\theta, t)}{\partial t}. \tag{44}$$

Therefore, substituting $\tilde{v}_r$ in equations (30) and (31) into equation (44), one can get the expression

$$X_n = \frac{\mathrm{i}A_n}{\omega R_0^2}[\tilde{x}_1\tilde{\alpha}_{1n}j_n'(\tilde{x}_1) + \tilde{x}_2\tilde{\alpha}_{2n}j_n'(\tilde{x}_2) + n(n+1)\tilde{\alpha}_{3n}j_n(\tilde{x}_3)], \tag{45}$$

where the symbol j_n' refers to the first derivative of the spherical Bessel function of first kind. Substituting the modal series solutions into the above boundary conditions, six

independent equations are obtained and can be cast into the following matrix form:

$$\begin{pmatrix} T_{11} & T_{12} & T_{13} & T_{14} & T_{15} & T_{16} \\ T_{21} & T_{22} & T_{23} & T_{24} & T_{25} & T_{26} \\ T_{31} & T_{32} & T_{33} & T_{34} & T_{35} & T_{36} \\ T_{41} & T_{42} & T_{43} & T_{44} & T_{45} & T_{46} \\ T_{51} & T_{52} & T_{53} & T_{54} & T_{55} & T_{56} \\ T_{61} & T_{62} & T_{63} & T_{64} & T_{65} & T_{66} \end{pmatrix} \begin{pmatrix} \alpha_1 \\ \alpha_2 \\ \alpha_3 \\ \tilde{\alpha}_1 \\ \tilde{\alpha}_2 \\ \tilde{\alpha}_3 \end{pmatrix} = \begin{pmatrix} M_1 \\ M_2 \\ M_3 \\ M_4 \\ M_5 \\ M_6 \end{pmatrix}. \tag{46}$$

The detailed expressions for the matrix elements are given in Appendix A. Because all the elements in matrices T and M are known, the unknowns $\alpha_{1,2,3}$, and $\tilde{\alpha}_{1,2,3}$ are completely determined. Then we can compute the scattering function and cross-section for all modes. First, the incident scalar potential for the plane wave is expanded as

$$\phi_I^{(1)} = \varepsilon e^{ik_1 z} = \varepsilon \sum_{n=0}^{\infty} i^n (2n+1) j_n(k_1 r) P_n(\cos\theta), \tag{47}$$

where ε is the incident wave amplitude. In the far field, the contribution of the scattering wave from thermal sound wave part is negligible, therefore, $|k_2 r| \gg |k_1 r| \gg 1$. Applying the asymptotic form for the spherical Hankel of first kind at $|k_1 r| \gg 1$,

$$h_n^{(1)}(k_1 r) \approx (-i)^{n+1} \frac{e^{ik_1 r}}{k_1 r} \tag{48}$$

to equation (27) and ignoring the contribution from $h_n^{(1)}(k_2 r)$ for the reason given above, the scattering wave is derived as

$$\phi_S^{(1)} = \varepsilon \frac{e^{ik_1 r}}{r} \sum_{n=0}^{\infty} \frac{-i(2n+1)\alpha_{1n} P_n(\cos\theta)}{k_1}. \tag{49}$$

Thus, the scattering function is derived as

$$f_s = \frac{-i}{k_1} \sum_{n=0}^{\infty} (2n+1)\alpha_{1n} P_n(\cos\theta), \tag{50}$$

and the total scattering cross-section is (see Appendix B)

$$\sigma_s = 4\pi R_0^2 \sum_{n=0}^{\infty} \frac{(2n+1)|\alpha_{1n}|^2}{|x_1|^2}. \tag{51}$$

For acoustic scattering by a bubble, equations (46), (50), and (51) present the *complete* solutions which incorporate the radiative, thermal, viscous, and surface tension effects on all modes for any frequency.

To compare the existing models which only considered the lowest vibrational mode, we consider the long-wavelength limit in the following. Under this condition, the pulsating mode $n = 0$ dominates, and the scattering function and cross-section are derived by keeping

the $n = 0$ term in equations (50) and (51), respectively:

$$f_0 = \frac{-i\alpha_{10}}{k_1}, \tag{52}$$

$$\sigma_{s0} = \frac{4\pi R_0^2 |\alpha_{10}|^2}{|x_1|^2}. \tag{53}$$

To derive the effective natural frequency and the damping constant, we cast equation (52) into a form similar to equation (1) and obtain

$$\omega_0^2 = \omega^2(1 + R_0 \,\mathrm{Re}[f_0^{-1}]), \tag{54}$$

and

$$\beta_T = \beta_a + \beta_v + \beta_t = -\frac{1}{2}\omega R_0 \,\mathrm{Im}[f_0^{-1}], \tag{55}$$

where $\mathrm{Re}[\cdot]$ indicates the real part and $\mathrm{Im}[\cdot]$ the imaginary part. Later we numerically compute each damping constant (radiative, viscous, and thermal damping) by turning off the other contributions.

2.2. DEVIN'S MODEL

The study of Devin [4] is a benchmark on the damping mechanisms of a pulsating bubble. He gave a rather concise review on the damping mechanism and on experimental methods determining the damping effects at resonance. The damping constants and natural frequency are analytically derived at resonance under several approximations. Specifically, in derivation of the thermal damping constant, Devin used the following main approximations. (1) Inside the bubble, both the density and pressure are assumed uniform (the inertia of gas are neglected) while keeping temperature inhomogeneous inside the bubble. (2) The temperature is constant at the gas–liquid interface (infinite thermal conductivity for the ambient liquid). Eller [5] further generalized Devin's arguments to examine the damping of a bubble driven both at resonance and away from resonance. Clay and Medwin recollected the results obtained by Eller in reference [1]. The derived results are summarized in Appendix C.

2.3. PROSPERETTI'S MODELS

2.3.1. *Model* I

In 1976, Prosperetti proposed a model on thermal effects and damping mechanisms in the forced oscillation of a gas bubble [2]. The author aimed at giving a straightforward approach and presented the results in analytically accessible forms. The complicated thermal interaction of the bubble with surrounding liquid was simplified by the polytropic equation of state for gas inside the bubble. The polytropic equation of state reads

$$P = \tilde{P}_0(R_0/R)^{3\kappa} - 4\mu_l \dot{R}/R, \tag{56}$$

TABLE 1

Summary of different models

Models	Devin [1, 4, 5]	Prosperetti I [2]	Prosperetti II [3]	Exact
β_a	$\dfrac{\omega^2 R_0}{2c_0}$	$\dfrac{\omega^2 R_0}{2c_0}$	$\dfrac{\omega^2 R_0}{2c_0}$	equation (55)
β_v	$\dfrac{2\mu_0}{\rho_0 R_0^2}$	$\dfrac{2\mu_0}{\rho_0 R_0^2}$	$\dfrac{2\mu_0}{\rho_0 R_0^2}$	equation (55)
β_t	equation (62)	equation (63)	equation (66)	equation (55)
Approximations made				
Modes considered	Pulsatory	Pulsatory	Pulsatory	All modes
Pressure inside the bubble	Uniform	Non-uniform	Uniform	Non-uniform
Bubble surface temperature	Fixed	Fixed	Fixed	Changable
Equation of state for gas	Ideal	Polytropic	Polytropic	Ideal

where P is the instantaneous pressure of the gas inside the bubble, R is the instantaneous bubble radius, μ_t is the effective viscosity caused by thermal dissipation, and κ is the effective polytropic exponent ranging from 1, representing an isothermal process, to $\tilde{\gamma}_0$ for the adiabatic process. It is shown that both the effective polytropic exponent and thermal damping constant depend on the driving frequency of incident pressure wave. The derived formulas are collected in Appendix C.

2.3.2. *Model* II

Later, Prosperetti *et al*. published another paper on the non-linear bubble dynamics [3]. After a careful order of magnitude analysis, the authors made the following assumptions. (1) The pressure is spatially uniform inside the bubble. (2) The bubble wall temperature remains unperturbed. Then, in the limit of small amplitude, they linearized the governing hydrodynamic equations. The results are also summarized in Appendix C.

2.4. SUMMARY OF DIFFERENT MODELS

For the sake of the reader's convenience, we summarize the different models in Table 1.

3. COMPARISON AND NUMERICAL RESULTS

We now proceed to compare numerical results for the different models. We use the following convention: "Devin" refers to Delvin's model, "Prosperetti I" refers to Prosperetti's first model, "Prosperetti II" refers to Prosperetti *et al*.'s second model, and the abbreviation "Exact" refers to the present theory.

First, the frequency response of the scattering cross-section, damping constant, and effective natural frequency are compared for different bubble sizes with particular attention paid to the thermal damping because of its importance in the energy dissipation. Then we examine the scattering properties at resonance for various bubble sizes. In the present theory, the normalized scattering cross-section is numerically obtained from equation (51),

while the cross-section from other models can be equivalently written in the form

$$\sigma_s = 4\pi R_0^2 \omega^4 / [\omega_0^2 - \omega^2)^2 + 4\beta_T^2 \omega^2], \tag{57}$$

with β_T and ω_0 being given above respectively. In this section, we discuss the special case of an air bubble in water. The parameters used for water at room temperature and one atmosphere are:

$$P_0 = 1{\cdot}01 \times 10^5 \text{ N/m}^2,\ T_0 = 298 \text{ K},\ \rho_0 = 1000\ kg/m^3,\ \kappa_0 = 0{\cdot}58 \text{ J/(s m K)},\ \mu_0 = 10^{-3} \text{ Pa s},$$

$$C_{p,0} = 4000 \text{ J/kg K},\ \gamma_0 = 1{\cdot}007,\ \alpha_0 = 2{\cdot}1 \times 10^{-4} \text{ K}^{-1},\ c_0 = 1485 \text{ m/s}.$$

For air,

$$\tilde{\kappa}_0 = 0{\cdot}034 \text{ J/(m s K)},\ \tilde{\mu}_0 = 1{\cdot}8 \times 10^{-5} \text{ Pa s},\ \tilde{C}_{p,0} = 1000 \text{ J/kg K},$$

$$\tilde{\gamma}_0 = 1{\cdot}40,\ \tilde{\alpha}_0 = 3{\cdot}3 \times 10^{-3}\, K^{-1},\ M = 28{\cdot}9 \times 10^{-3} \text{ kg},$$

and the surface tension for air–water interface,

$$\sigma = 0{\cdot}073 \text{ kg/s}^2.$$

Moreover, the adiabatic sound speed and air density inside the bubble are determined from the ideal gas equation of state as

$$\tilde{\rho}_0 = \frac{\tilde{P}_0 M}{R_g T_0},\ \tilde{c}_0 = \sqrt{\frac{\tilde{\gamma}_0 \tilde{P}_0}{\tilde{\rho}_0}}, \tag{58}$$

with

$$\tilde{P}_0 = P_0 + \frac{2\sigma}{R_0}.$$

In Figure 1, the plots for the reduced scattering cross-section versus frequency in the Rayleigh scattering and geometric regimes are shown for the case of bubble radius $R_0 = 10$ μm respectively. From these figures, we observe the following. In low-frequency limit (i.e., Rayleigh regime), we observed that all the models and ours satisfied the Rayleigh scattering relation ($\sigma_s \propto \omega^4$). However, Devin's model is only qualitatively correct and predicts a much smaller scattering cross-section.

At the high-frequency end (i.e., geometric regime), our results deviate from the other three models. The reason is that the high order vibrational modes of the bubble become important at the high-frequency end, and thus the other models merely based on the pulsating mode are no longer valid. Hereafter, we define a critical frequency as the frequency above which the response of the bubble cannot be represented by the pulsating mode only with the error tolerance of 10%. For $R_0 = 10$ μm, the high order modes are not negligible above the critical frequency $\omega_{c1} = 6 \times 10^7$ (1/s). For $R_0 = 100$ and 1 μm cases not shown here, the derived critical frequencies are $\omega_{c2} = 6 \times 10^6$ (1/s) and $\omega_{c3} = 6 \times 10^8$ (1/s) respectively. In later discussions, we will restrict our attention to the frequency regime in which pulsating mode dominates. Second, the discrepancies between these models also exist near the resonance for these sizes. Therefore, the calculated natural frequency and damping constants from these models may differ.

To show the difference near resonant scattering, we present the results in Figure 2. From these figures, we observe the following features. (1) The results from "Devin" and

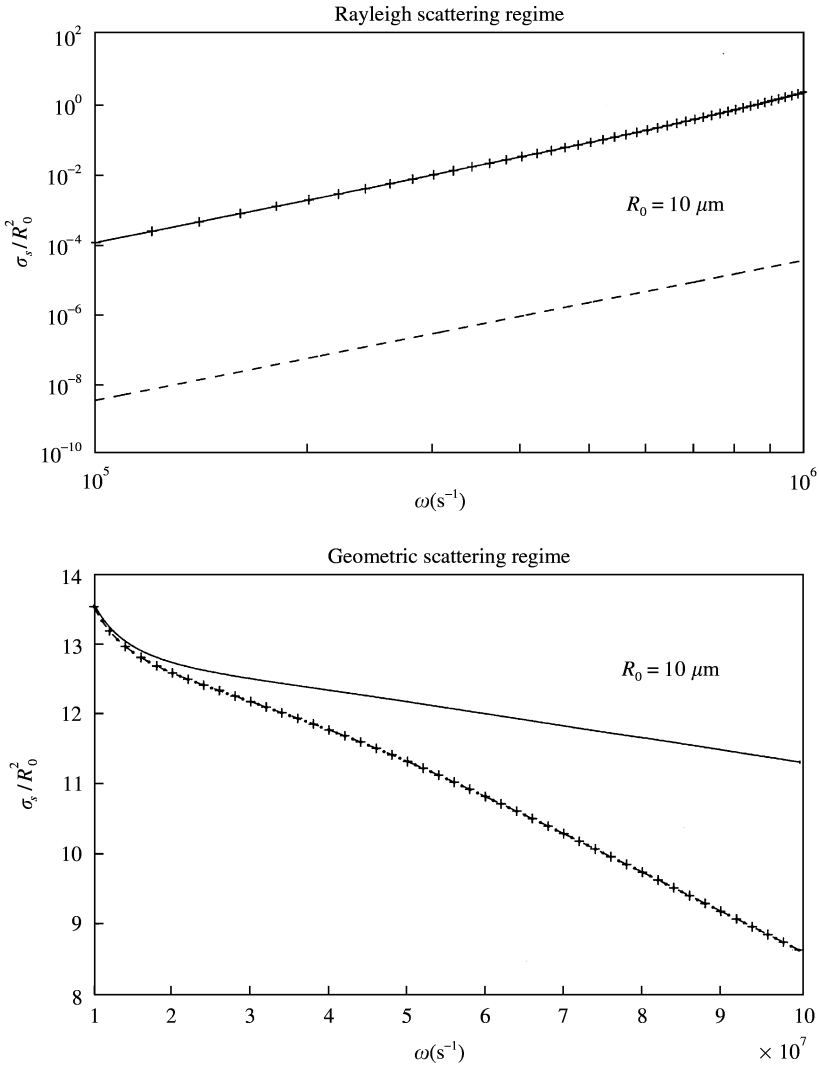

Figure 1. Reduced scattering cross-section versus frequency: ——, Exact; +, Prosperetti II; ·, Prosperetti I; – – – – – –, Devin.

"Prosperetti I" are in good agreement with that from "Exact" only for large bubble sizes, such as $R_0 = 100\ \mu$m. For $R_0 = 10$, 1 μm, "Devin" and "Prosperetti I" overestimate the scattering cross-section by 5·5 and 5% compared to "Exact" respectively. (2) "Prosperetti II" and "Exact" are in good agreement in all these cases.

To search for reasons of the differences between these models, we examine the effective natural frequency and the thermal damping constant in Figures 3 and 4 separately. In Figure 3, the plots of the effective natural frequency versus angular frequency are shown for $R_0 = 100$, 10 and 1 μm. We notice that the effective natural frequency increases monotonically with frequency for all these bubble sizes. We show that all the effective natural frequencies from "Prosperetti II", "Prosperetti I", and "Devin" agree fairly well for the entire frequency range. It is also noticed that the results from "Exact" coincide with that from these models only for frequencies below the resonance. Differences are only observed

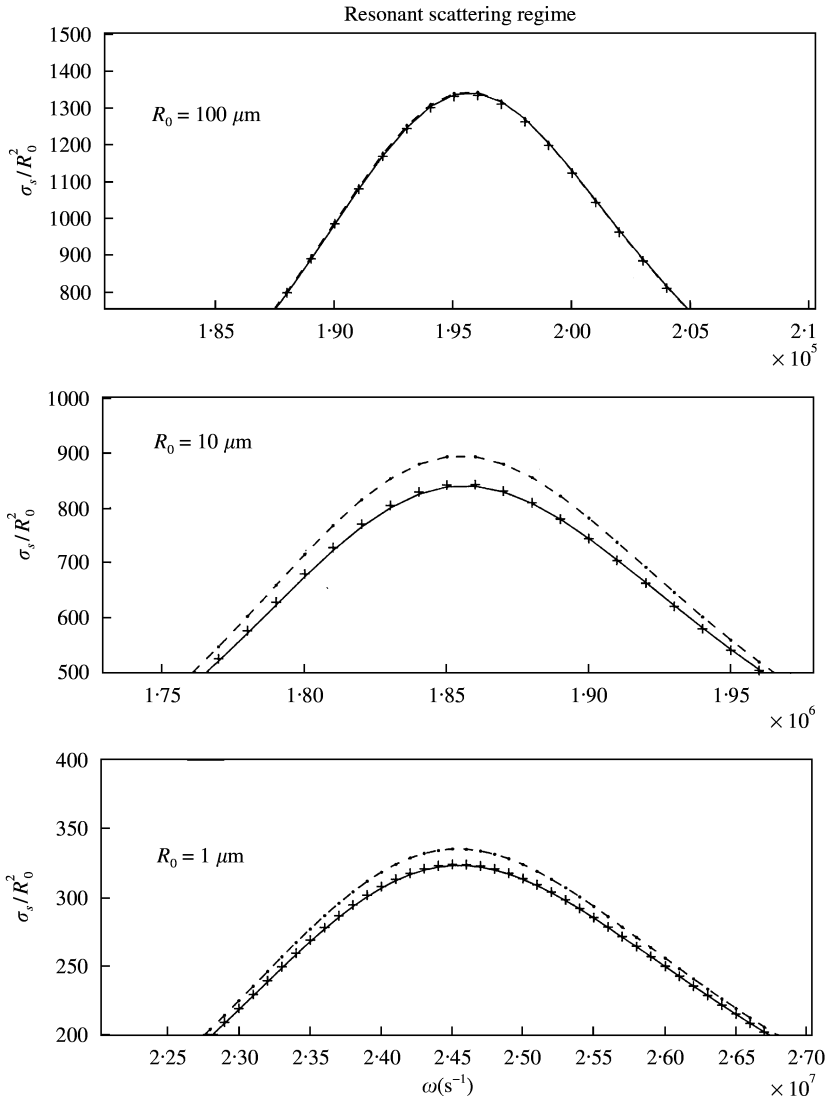

Figure 2. Reduced scattering cross-section near resonance: ——, Exact; +, Prosperetti II; · , Prosperetti I; – – – – – –, Devin.

for the frequencies above the resonance and are prominent for smaller bubble size in these figures. A reason for the discrepancy is that is their models the gas inertial effect is not considered. When the effect is taken into account, the assumption that the pressure is uniform inside the bubble is no longer valid. At high frequencies, there is not enough time for the air to distribute uniformly inside the bubble. As a result, the actual internal energy of the air is higher than that assumed in the uniform state, thereby yielding a higher effective natural frequency than in the uniform assumption. Indeed, we observe that by reducing the gas density, the curves from "Exact" are getting closer and closer to that of other models.

In Figure 4, the plots of the thermal damping constant versus frequency are exhibited. We observe the following features. First, the thermal damping constant from "Prosperetti II" is in good agreement with that from "Exact" for $R_0 = 100$, 10 and 1 μm. Second, "Devin" and

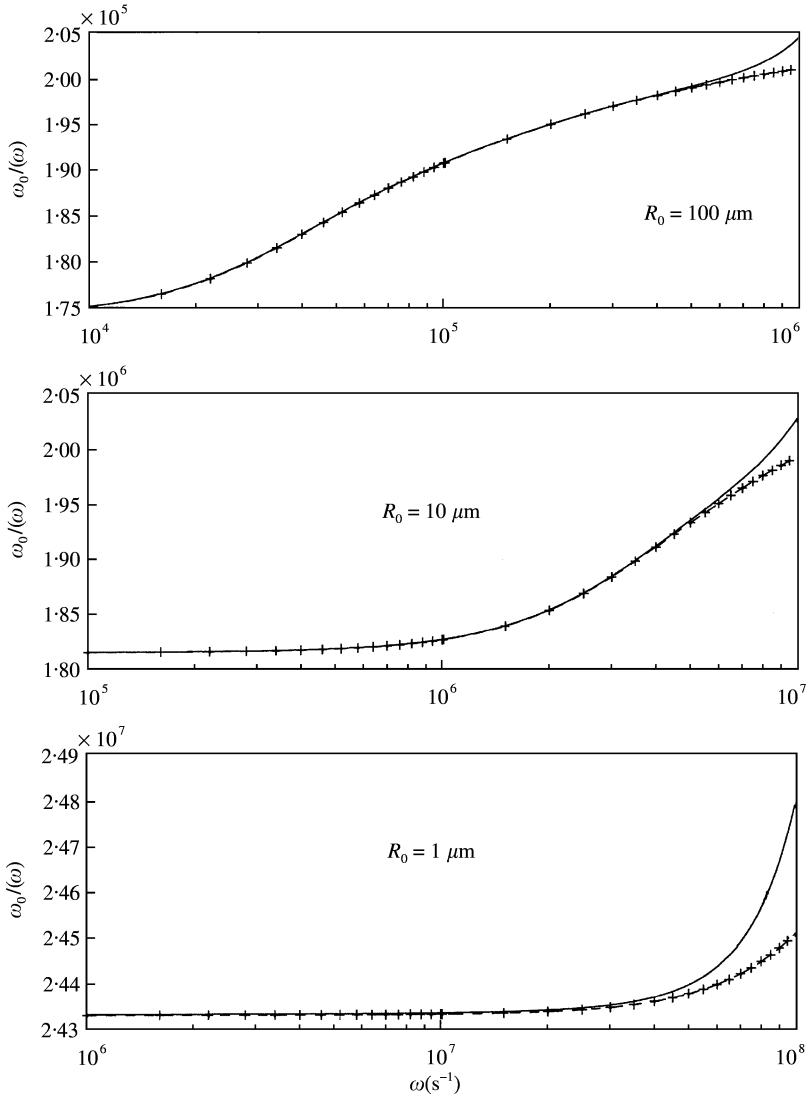

Figure 3. Effective natural frequency versus frequency: ——, Exact; +, Prosperetti II; · , Prosperetti I; – – – – – –, Devin.

"Prosperetti I" underestimate the thermal damping constant, and the difference becomes larger for smaller bubble size. We also examine the viscous damping and radiative damping constants from these models, yielding good agreements. From these comparisons, we arrive at the following conclusions. (1) The previous three models are no longer valid for higher frequencies at which the higher order modes in the bubble's oscillation become dominant. (2) "Devin" underestimates the scattering cross-section in Rayleigh scattering regime. (3) These models only agree with each other for large bubble size up to $R_0 = 100$ μm. (4) The previous three models do not predict the correct thermal damping constant for frequencies ranging between the resonant frequency and critical frequency.

For practical interest, we now examine the scattering properties at resonance for the bubble radius ranging from 1 to 100 μm. In Figure 5, the plot of the normalized scattering

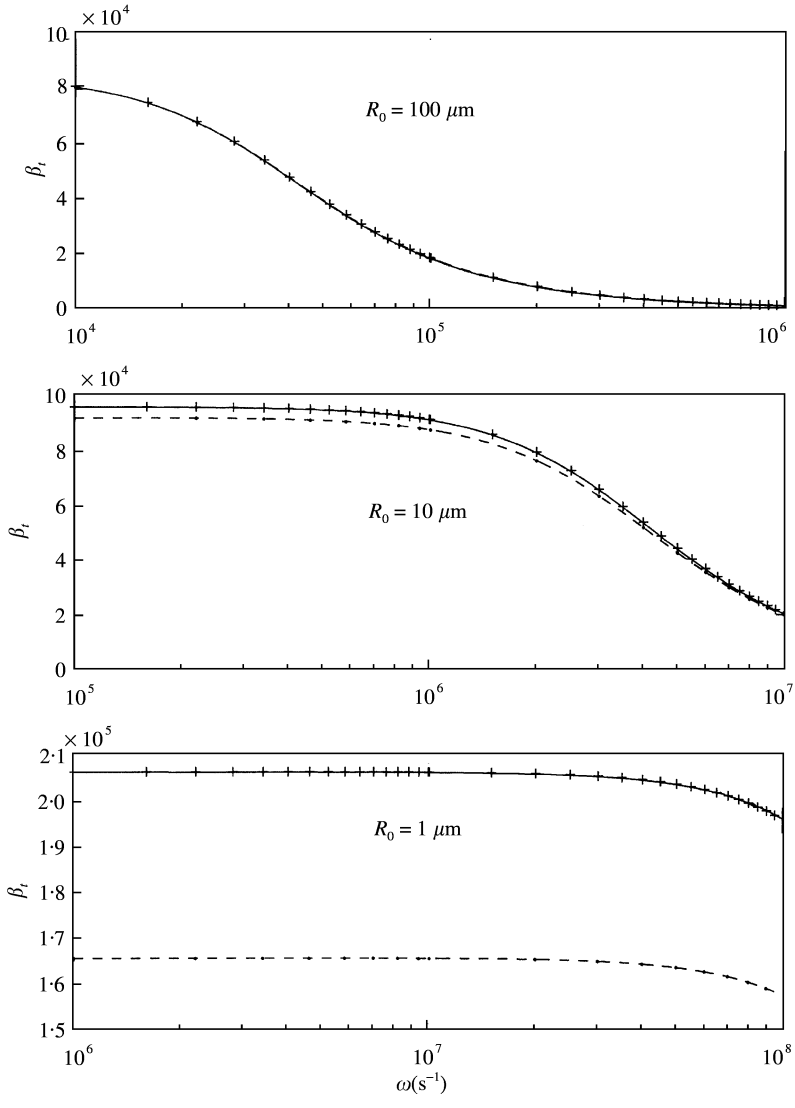

Figure 4. Thermal damping constant versus frequency: ——, Exact; +, Prosperetti II; ·, Prosperetti I; – – – – – –, Devin.

cross-section at resonance as a function of bubble radius is shown for different models. The following features are observed. First, only "Prosperetti I" predicts a monotonically increasing curve, in contrast to the other predictions. Second, "Devin" overestimates the resonant scattering cross-section (RSCS) for bubbles smaller than 50 μm. Third, results from "Prosperetti II" are in reasonably good agreement with that from "Exact".

In Figure 6, the thermal damping constant at resonance as a function of bubble radius is displayed. We notice that the thermal damping constant decreases monotonically with the bubble radius for all models. "Prosperetti I" overestimates the thermal damping constant, while "Devin" underestimates that for bubble sizes less than 10 μm. Once again, the thermal damping constant from "Prosperetti II" is in good accordance with the exact solution.

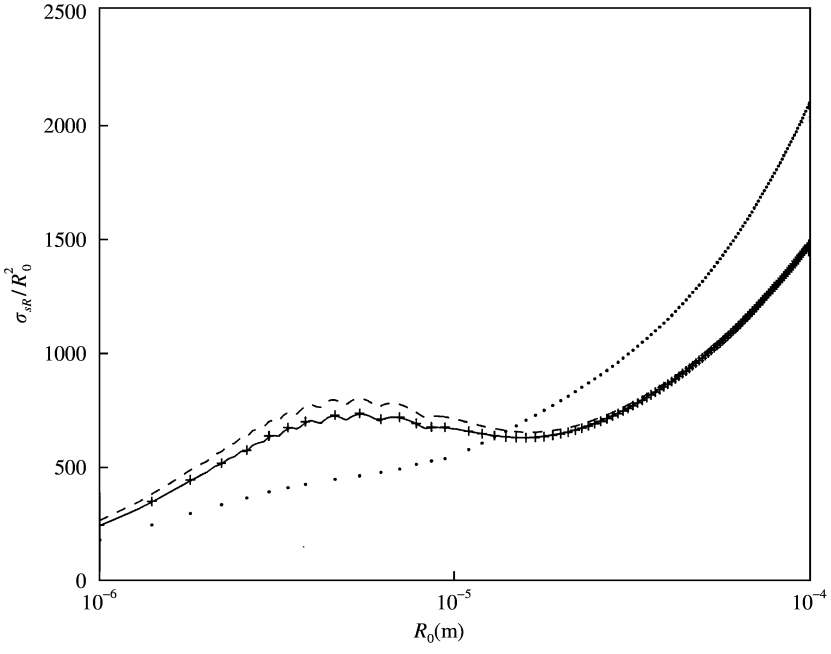

Figure 5. Reduced resonant scattering cross-section versus bubble radius: ——, Exact; +, Prosperetti II; ·, Prosperetti I; – – – – – –, Devin.

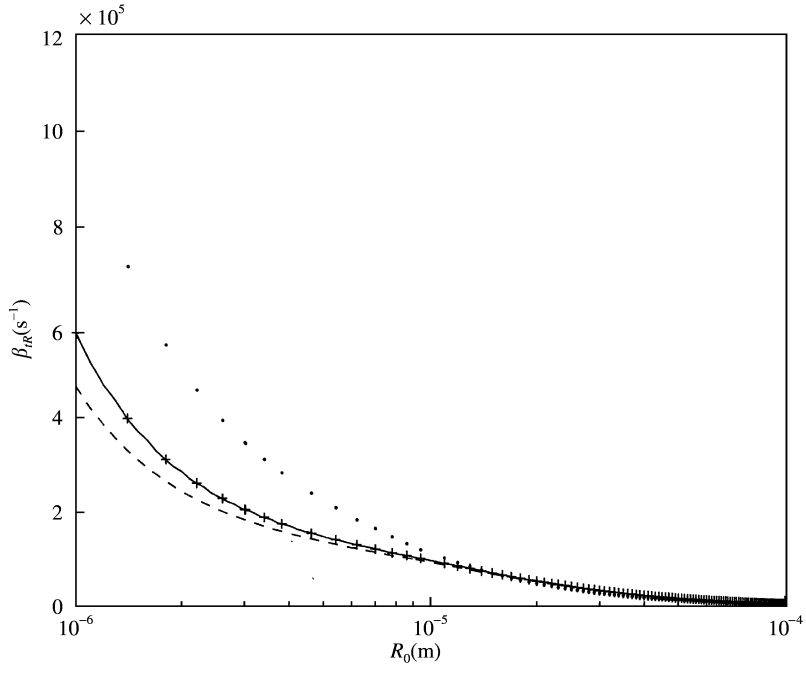

Figure 6. Thermal damping constant at resonance versus bubble radius: ——, Exact; +, Prosperetti II; ·, Prosperetti I; – – – – – –, Devin.

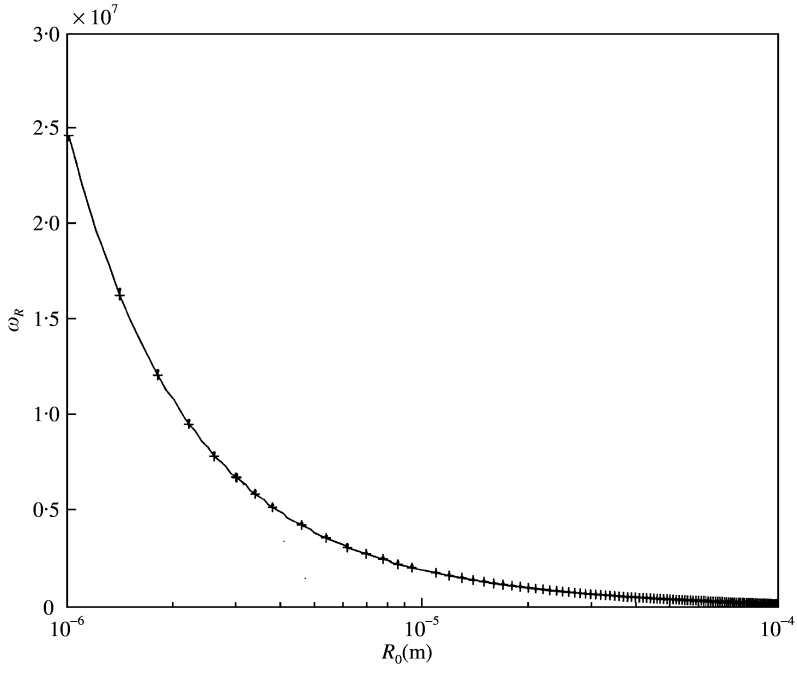

Figure 7. Resonant frequency versus bubble radius: ——, Exact; +, Prosperetti II; · , Prosperetti I; – – – – –, Devin.

In Figure 7, we show the resonant frequency versus bubble radius. It is noticed that the resonant frequency decreases with the bubble radius for all models. And the results from these models agree with each other fairly well. From the above discussion at resonance, we arrive at the following conclusion. First, the previous models can predict the accurate resonant frequency position for different bubble sizes. Second, "Devin" overestimates the RSCS and predicts a resonant peak with higher Q (quality factor) for bubble radius smaller than 50 μm. Third, the RSCS predicted by "Prosperetti I" would be underestimated for bubbles smaller than $R_0 = 15\,\mu$m and overestimated for bubbles larger than that. Moreover, lower Q peaks are predicted for small bubble size. Fourth, "Prosperetti II" is in excellent agreement with out results at resonance.

4. CONCLUSION

In this paper, we first derived an exact solution for sound scattering by an air bubble in water for all modes. By applying to the cases corresponding to different scattering regimes, we then compared the acoustic scattering properties with that obtained from Devin's and Prosperetti's approaches. The following remarkable results are drawn. In the Rayleigh scattering regime, we show that "Devin" will greatly underestimate the scattering cross-section for bubble sizes considered in this paper while the others show good agreement with "Exact" quantitatively. In the geometric scattering regime, it was shown that the previous models are no longer applicable above certain frequencies. For the cases of bubble radii $R_0 = 100$, 10 and 1 μm, the critical frequencies are 6×10^6, 6×10^7, and 6×10^8 (1/s) respectively. In the bubble's resonant regime, the limitations of previous works on thermal exchange process which is often masked by polytropic equation of state inside

the bubble have been shown. The conclusions are drawn as follows. (1) All models predict the accurate resonant peak position for all the bubble sizes. (2) "Devin" overestimates the RSCS and predicts a resonant peak with higher Q (quality factor) for bubble radius smaller than 50 μm. (3) The RSCS predicted from "Prosperetti I" would be underestimated for $R_0 < 15$ μm while being overestimated for larger bubbles. (4) "Prosperetti II" is in excellent agreement with "Exact" at resonance. In addition, the abnormal thermal exchange process for a bubble in water for frequencies above resonance is discussed. The fact that the present exact results match that from "Prosperetti II" not only provides a further justification of their approach, but also gives us confidence in our approach. The fair agreement shows that the model "Prosperetti II" is approximate, yet captures the essence of the physical process in the valid range of frequencies. The present results can be extended to a wide range of frequencies and to frequency ranges beyond the applicability of the previous approaches. From the derivation, it is also clear that the approach presented in this paper is also valid for any other fluid enclosures in liquids.

ACKNOWLEDGMENTS

Discussions with Dr Alberto Alvarez are acknowledged. One of the authors (CCW) also benefited from discussion with Dr C.-Y. Lu. The work received support from the National Science Council of ROC and the National Central University.

REFERENCES

1. C. S. Clay and H. Medwin 1977 *Acoustical Oceanography*. New York: Wiley.
2. A. Prosperetti 1977 *Journal of the Acoustical Society of America* **61**, 17–27. Thermal effects and damping mechanisms in the forced radial oscillations of gas bubbles in liquids.
3. A. Prosperetti, L. A. Crum and K. W. Commander 1988 *Journal of the Acoustical Society of America* **83**, 502–514. Nonlinear bubble dynamics.
4. C. Devin 1959 *Journal of the Acoustical Society of America* **31**, 1654. Survey of thermal, radiation, and viscous damping of pulsating air bubbles in water.
5. AI. Eller 1970 *Journal of the Acoustical Society of America* **47**, 1469. Damping constants of pulsating bubbles.
6. A. Prosperetti 1984 *Ultrasonics* **22**, 69. Bubble phenomena in sound fields: part one.
7. M. S. Plesset and D.-Y. Hseih 1960 *Physics of Fluids* **3**, 882. Theory of gas bubble dynamics in oscillating pressure fluids.
8. M. Minnaert 1933 *Philosophical Magazine* **26**, 235.
9. P. M. Morse and H. Feshbach 1953 *Method of Theoretical Physics*, Vol. II New York: MacGraw-Hill, Inc.
10. D. M. Farmer and D. Lemon 1984 *Journal of Physical Oceanography* **14**, 855–863. The influence of bubbles on ambient noise in the ocean at high wind speed.
11. Z. Ye 1996 *Journal of the Acoustical Society of America* **99**, 785–792. Acoustic scattering from fish swimbladders.
12. N. De Jong and L. Hoff 1993 Ultrasonics **31**, 175. Ultrasound scattering properties of Albunex Microspheres.
13. A. A. Doinikov 1997 *Journal of the Acoustical Society of America* **101**, 713–721. Acoustic radiation force on a spherical particle in a viscous heat-conducting fluid, I. General formula.
14. L. D. Landau and E. M. Lifshitz 1984 *Fluid Mechanics*. New York: Butterworth-Heinemann; second edition.
15. A. A. Doinikov 1997 *Journal of the Acoustical Society of America* **101**, 731–740. Acoustic radiation force on a spherical particle in a viscous heat-conducting fluid, III. Force on a liquid drop.
16. K. Huang 1987 *Statistical Mechanics*, 19–22. New York: John Wiley and Sons; second edition.

APPENDIX A

$$x_1 = k_1 R_0,\ x_2 = k_2 R_0,\ x_3 = k_3 R_0,\ \tilde{x}_1 = \tilde{k}_1 R_0,\ \tilde{x}_2 = \tilde{k}_2 R_0,\ \tilde{x}_3 = \tilde{k}_3 R_0.$$

$$\lambda_p = \frac{\rho_0}{\tilde{\rho}_0},\ \lambda_\mu = \frac{\mu_0}{\tilde{\mu}_0},\ \lambda_\beta = \frac{\beta_3}{\tilde{\beta}_3},\ \lambda_\alpha = \frac{\alpha_0}{\tilde{\alpha}_0},\ \lambda_\kappa = \frac{\kappa_0}{\tilde{\kappa}_0}.$$

A.1. MATRIX ELEMENTS OF T

$$T_{11} = x_1 h_n^{(1)'}(x_1), \qquad T_{12} = x_2 h_n^{(1)'}(x_2), \qquad T_{13} = n(n+1) h_n^{(1)}(x_3),$$

$$T_{14} = -\tilde{x}_1 j_n'(\tilde{x}_1), \qquad T_{15} = -\tilde{x}_2 j_n'(\tilde{x}_2), \qquad T_{16} = -n(n+1) j_n(\tilde{x}_3),$$

$$T_{21} = h_n^{(1)}(x_1), \qquad T_{22} = h_n^{(1)}(x_2), \qquad T_{23} = x_3 h_n^{(1)'}(x_3) + h_n^{(1)}(x_3),$$

$$T_{24} = -j_n(\tilde{x}_1), \qquad T_{25} = -j_n(\tilde{x}_2), \qquad T_{26} = -[\tilde{x}_3 j_n'(\tilde{x}_3) + j_n(\tilde{x}_3)],$$

$$T_{31} = \frac{\lambda_\beta}{\lambda_\alpha} h_n^{(1)}(x_1), \qquad T_{32} = \frac{\lambda_\beta}{\lambda_\alpha}\left(\frac{\beta_1 - k_2^2}{\beta_1 - k_1^2}\right) h_n^{(1)}(x_2), \qquad T_{33} = 0,$$

$$T_{34} = -\left(\frac{\tilde{\beta}_1 - \tilde{k}_1^2}{\beta_1 - k_1^2}\right) j_n(\tilde{x}_1), \qquad T_{35} = -\left(\frac{\tilde{\beta}_1 - \tilde{k}_2^2}{\beta_1 - k_1^2}\right) j_n(\tilde{x}_2), \qquad T_{36} = 0,$$

$$T_{41} = x_1 h_n^{(1)'}(x_1), \qquad T_{42} = \left(\frac{\beta_1 - k_2^2}{\beta_1 - k_1^2}\right) x_2 h_n^{(1)'}(x_2),$$

$$T_{43} = 0, \qquad T_{44} = -\frac{\lambda_\alpha}{\lambda_\beta \lambda_\kappa}\left(\frac{\tilde{\beta}_1 - \tilde{k}_1^2}{\beta_1 - k_1^2}\right) \tilde{x}_1 j_n'(\tilde{x}_1),$$

$$T_{45} = -\frac{\lambda_\alpha}{\lambda_\beta \lambda_\kappa}\left(\frac{\tilde{\beta}_1 - \tilde{k}_2^2}{\beta_1 - k_1^2}\right) \tilde{x}_2 j_n'(\tilde{x}_2), \qquad T_{46} = 0,$$

$$T_{51} = x_1 h_n^{(1)'}(x_1) - \frac{1}{2}\left[n(n+1) + \frac{\lambda_\rho \tilde{x}_3^2}{2(1-\lambda_\mu)}\right] h_n^{(1)}(x_1),$$

$$T_{52} = x_2 h_n^{(1)'}(x_2) - \frac{1}{2}\left[n(n+1) + \frac{\lambda_\rho \tilde{x}_3^2}{2(1-\lambda_\mu)}\right] h_n^{(1)}(x_2),$$

$$T_{53} = \frac{1}{2} n(n+1)[h_n^{(1)}(x_3) - x_3 h_n^{(1)'}(x_3)],$$

$$T_{54} = \frac{\tilde{x}_3^2}{4(1-\lambda_\mu)}\left[j_n(\tilde{x}_1) - \frac{\sigma(n-1)(n+2)}{\omega^2 R_0^3 \tilde{\rho}_0} \tilde{x}_1 j_n'(\tilde{x}_1)\right],$$

$$T_{55} = \frac{\tilde{x}_3^2}{4(1-\lambda_\mu)}\left[j_n(\tilde{x}_2) - \frac{\sigma(n-1)(n+2)}{\omega^2 R_0^3 \tilde{\rho}_0} \tilde{x}_2 j_n'(\tilde{x}_2)\right],$$

$$T_{56} = -\frac{\tilde{x}_3^2}{4(1-\lambda_\mu)} \frac{\sigma(n-1)n(n+1)(n+2)}{\omega^2 R_0^3 \tilde{\rho}_0} j_n(\tilde{x}_3),$$

$$T_{61} = h_n^{(1)}(x_1) - x_1 h_n^{(1)'}(x_1), \qquad T_{62} = h_n^{(1)}(x_2) - x_2 h_n^{(2)'}(x_2),$$

$$T_{63} = \left[n(n+1) - 1 + \frac{\lambda_\rho \tilde{x}_3^2}{2(1-\lambda_\mu)} \right] h_n^{(1)}(x_3) - x_3 h_n'^{(1)}(x_3),$$

$$T_{64} = 0, \qquad T_{65} = 0, \qquad T_{66} = -\frac{\tilde{x}_3^2}{2(1-\lambda_\mu)} j_n(\tilde{x}_3).$$

A.2. MATRIX ELEMENTS OF M

$$M_1 = -x_1 j_n'(x_1),\ M_2 = -j_n(x_1),\ M_3 = -\frac{\lambda_\beta}{\lambda_\alpha} j_n(x_1),\ M_4 = -x_1 j_n'(x_1),$$

$$M_5 = -\{x_1 j_n'(x_1) - \frac{1}{2}\left[n(n+1) + \frac{\lambda_\rho \tilde{x}_3^2}{2(1-\lambda_\mu)} \right] j_n(x_1)\},$$

$$M_6 = -[\, j_n(x_1) - x_1 j_n'(x_1)].$$

APPENDIX B

B.1. CALCULATION OF SCATTERING CROSS-SECTION

The scattering cross-section is related with scattering function by

$$\sigma_s = \int |f_s(\theta)|^2 \, \mathrm{d}\Omega.$$

With the aid of the orthogonal relation for Legendre polynomial

$$\int_{-1}^{1} P_n(x) P_{n'}(x) \, \mathrm{d}x = \frac{2}{2n+1} \delta_{nn'},$$

where $x = \cos\theta$, Ω is the solid angle, and

$$\delta_{nn'} = 1, \quad \text{if } n = n',$$

$$\delta_{nn'} = 0, \quad \text{if } n \neq n',$$

the scattering cross-section in equation (51) is derived.

APPENDIX C

C.1. DEVIN'S MODEL

The natural frequency is given by

$$\omega_0 = \frac{1}{R_0} \left(\frac{3\tilde{\gamma}_0 b \beta P_0}{\tilde{\rho}_0} \right)^{1/2}, \tag{C.1}$$

where $\tilde{\rho}_0$ is the gas density, $\tilde{\gamma}_0$ is the gas specific heat ratio, and P_0 is the equilibrium pressure in the ambient liquid, and

$$\beta = 1 + \frac{2\sigma}{P_0 R_0}\left(1 - \frac{1}{3\tilde{\gamma}_0 b}\right), \quad X = R_0\left(\frac{2\omega\tilde{\rho}_0\tilde{C}_{p,0}}{\tilde{\kappa}_0}\right)^{1/2}$$

$$b = \left[1 + \left(\frac{d}{b}\right)^2\right]^{-1}\left[\frac{3(\tilde{\gamma}_0 - 1)}{X}\frac{\sinh X - \sin X}{\cosh X - \cos X}\right]^{-1}$$

in which $\tilde{\kappa}_0$ is the gas thermal conductivity, $\tilde{C}_{p,0}$ is the gas specific heat at constant pressure. The viscous damping constant is derived as

$$\beta_v = 2\mu_0/(\rho_0 R_0^2), \tag{C.2}$$

the acoustic radiation damping constant is given by

$$\beta_a = \frac{\omega^2 R_0}{2c_0}, \tag{C.3}$$

and the thermal damping constant is represented as

$$\beta_t = \frac{d}{2b}\,\omega\left(\frac{\omega_0}{\omega}\right)^2. \tag{C.4}$$

In the above, d/b is given by

$$\frac{d}{b} = 3(\tilde{\gamma}_0 - 1)\left[\frac{X(\sinh X + \sin X) - 2(\cosh X - \cos X)}{X^2(\cosh X - \cos X) + 3(\tilde{\gamma}_0 - 1)X(\sinh X - \sin X)}\right].$$

C.2. PROSPERETTI'S MODELS

Model I

In this model, the analytical forms for the viscous and radiative damping constants are identical to that in Devin's model. The thermal damping constant, however, is given by

$$\beta_t = \tfrac{1}{2}(\tilde{\rho}_0\omega/\rho_0)\,\mathrm{Im}(\phi), \tag{C.5}$$

the effective polytropic exponent is written as

$$\kappa = (\tilde{\gamma}_0/3)G_1 G_2\,\mathrm{Re}(\phi), \tag{C.6}$$

and the effective natural frequency is derived as

$$\omega_0^2 = 3\kappa\tilde{P}_0/\rho_0 R_0^2 - 2\sigma/\rho_0 R_0^3 + (\omega R_0/c_0)^2[1 + (\omega R_0/c_0)^2]^{-1}\omega^2 \tag{C.7}$$

with

$$G_1 = M\omega\tilde{D}_{v,0}/\tilde{\gamma}_0 R_g T_0, \quad G_2 = \omega R_0^2/\tilde{D}_{v,0},$$

and

$$\phi = \frac{kf(\Gamma_2 - \Gamma_1) + \lambda_2\Gamma_2 - \lambda_1\Gamma_1}{kf(\lambda_2\Gamma_1 - \lambda_1\Gamma_2) - \lambda_1\lambda_2(\Gamma_2 - \Gamma_1)},$$

where M is the molecular weight of the gas within the bubble, $\tilde{C}_{v,0}$ is the gas specific heat at constant volume, $\tilde{D}_{v,0} = \tilde{\kappa}_0/\tilde{\rho}_0\tilde{C}_{v,0}$ is the gas thermal diffusivity, R_g is the universal gas constant, T_0 is the absolute equilibrium temperature of the surrounding liquid, and $k = \kappa_0/\tilde{\kappa}_0$ is the thermal conductivity ratio of the liquid to gas. In the above,

$$\Gamma_{1,2} = \mathrm{i} + G_1 \pm [(\mathrm{i} - G_1)^2 + 4\mathrm{i}G_1/\tilde{\gamma}_0]^{1/2},$$

$$\lambda_{1,2} = \beta_{1,2}\coth(\beta_{1,2}) - 1,$$

$$\beta_{1,2} = (\tfrac{1}{2}\tilde{\gamma}_0 G_2\{\mathrm{i} - G_1 \pm [(\mathrm{i} - G_1)^2 + 4\mathrm{i}G_1/\tilde{\gamma}_0]^{1/2}\})^{1/2},$$

$$f = 1 + (1 + \mathrm{i})(\tfrac{1}{2}G_3)^{1/2}, \quad G_3 = \omega R_0^2/D_{v,0}$$

where $D_{v,0} = \kappa_0/\rho_0 C_{v,0}$ is the thermal diffusivity of the surrounding liquid.

Model II

In this model, the calculated radiative and viscous damping constants remain unchanged, while the revised thermal damping constant is given by

$$\beta_t = \frac{\tilde{P}_0}{2\rho_0\omega R_0^2}\,\mathrm{Im}\Phi, \tag{C.8}$$

and the effective natural frequency is derived as

$$\omega_0^2 = \frac{\tilde{P}_0}{\rho_0 R_0^2}\left(\mathrm{Re}\,\Phi - \frac{2\sigma}{R_0\tilde{P}_0}\right), \tag{C.9}$$

with

$$\Phi = \frac{3\tilde{\gamma}_0}{1 - 3(\tilde{\gamma}_0 - 1)\mathrm{i}\chi_g[(\mathrm{i}/\chi_g)^{1/2}\coth(\mathrm{i}/\chi_g)^{1/2} - 1]}, \quad \chi_g = \tilde{D}_{p,0}/\omega R_0^2, \tag{C.10}$$

where $\tilde{D}_{p,0} = \tilde{\kappa}_0/\tilde{\rho}_0\tilde{C}_{p,0}$ is the thermal diffusivity of gas at constant pressure.